Rapid Communications

Elementary plastic events in amorphous silica

Silvia Bonfanti,[1] Roberto Guerra,[1] Chandana Mondal,[2] Itamar Procaccia,[2,3] and Stefano Zapperi[1,4]

[1]*Center for Complexity and Biosystems, Department of Physics, University of Milan, via Celoria 16, 20133 Milano, Italy*

[2]*Department of Chemical Physics, Weizmann Institute of Science, Rehovot 76100, Israel*

[3]*Center for Optical Imagery Analysis and Learning, Northwestern Polytechnical University, Xi'an 710072, China*

[4]*CNR (Consiglio Nazionale delle Ricerche), Istituto di Chimica della Materia Condensata e di Tecnologie per l'Energia, Via R. Cozzi 53, 20125 Milano, Italy*

(Received 24 October 2019; published 23 December 2019)

Plastic instabilities in amorphous materials are often studied using idealized models of binary mixtures that do not capture accurately molecular interactions and bonding present in real glasses. Here we study atomic-scale plastic instabilities in a three-dimensional molecular dynamics model of silica glass under quasistatic shear. We identify two distinct types of elementary plastic events, one is a standard quasilocalized atomic rearrangement while the second is a bond-breaking event that is absent in simplified models of fragile glass formers. Our results show that both plastic events can be predicted by a drop of the lowest nonzero eigenvalue of the Hessian matrix that vanishes at a critical strain. Remarkably, we find very high correlation between the associated eigenvectors and the nonaffine displacement fields accompanying the bond-breaking event, predicting the locus of structural failure. Both eigenvectors and nonaffine displacement fields display an Eshelby-like quadrupolar structure for both failure modes, rearrangement, and bond breaking. Our results thus clarify the nature of atomic-scale plastic instabilities in silica glasses, providing useful information for the development of mesoscale models of amorphous plasticity.

DOI: 10.1103/PhysRevE.100.060602

Introduction. Amorphous solids under applied shear deformation undergo localized plastic instabilities associated with the rearrangement of a subset of particles and an associated energy release. These particle reorganization induces structural deformation patterns that have been identified experimentally and numerically in amorphous materials such as silica glasses [1–3], metallic glasses [4], colloidal glasses [5], foams [6], bubble rafts [4], and emulsions [7,8]. The initial destabilization can give rise to a progression of additional deformation events in some other areas of the sample, up to the global material failure. The ability to predict the plastic instabilities and characterize their spatial features is of fundamental importance to understanding the mechanical response of amorphous solids and to devise mesoscale model focusing on the evolution of localized plastic events [9–12].

A useful theoretical framework for analyzing elementary plastic events is the limit of temperature $T = 0$ and of quasistatic strain where the real space structure can be easily related with a potential energy landscape description [13]. To this end, many computational studies on amorphous solids have been performed with athermal quasistatic (AQS) protocol [14–18]: A glass sample initially quenched down to zero temperature is deformed by a quasistatic shear procedure consisting of the relaxation of the system after each strain step. Within the AQS conditions, the elastic and plastic features of amorphous solids can be understood by analyzing the Hessian matrix

$$H_{ij} \equiv \frac{\partial^2 U(\boldsymbol{r}_1, \ldots, \boldsymbol{r}_N)}{\partial \boldsymbol{r}_i \partial \boldsymbol{r}_j} \equiv -\frac{\partial \boldsymbol{f}_i(\boldsymbol{r}_1, \ldots, \boldsymbol{r}_N)}{\partial \boldsymbol{r}_j}, \qquad (1)$$

where $U(\boldsymbol{r}_1, \boldsymbol{r}_2, \ldots \boldsymbol{r}_N)$ is the total potential energy of the system, $\boldsymbol{f}_i$ is the force vector on particle i, and $\{\boldsymbol{r}_i\}_{i=1}^N$ are the coordinates of the particles. The explicit $\boldsymbol{H}$ element expression is reported in Ref. [19]. When the system is mechanically stable, the eigenvalues λ of the Hessian are semipositive, with zero values for the Goldstone modes and all the rest positive. Elementary plastic instabilities are signaled by the lowest eigenvalue $\lambda_{\min}$ going to zero and an eigenfunction getting quasilocalized on a pattern correlated with real space nonaffine displacements. Typically observed quadrupole-like structure can be described as an ellipsoidal inclusion in an elastic medium [20], following the classic work of Eshelby [21]. This kind of analysis always gives rise to a similar phenomenology, independent of the detailed microscopic interactions between the constituents [17], but to the best of our knowledge it has only be applied to idealized model of fragile glasses [22] such as metallic glasses [17,23,24] or frictional disks whose packing structure is isotropic [25,26].

Experimental evidences of atomic rearrangements for two-dimensional silica glass have been reported in Ref. [3], while numerically the plastic rearrangements in strained silica at zero temperature have been investigated in Ref. [27]. We are lacking, however, numerical studies of normal modes in realistic strong glass formers such as silica that are characterized by a strong chemical structural order with tetrahedral networks made by covalent bonds. Indeed, silica glass is appealing not only for technological and commercial applications but also for its intriguing and anomalous behavior that is still not fully understood. In particular, we mention here the peaks in the specific heat, the diffusion constant, the density maximum [28], and so on, that differentiates silica from all other fragile glasses. Therefore, *a priori,* the nature of plastic instabilities in silica glasses is not clear, especially considering the relevance of *anisotropic*

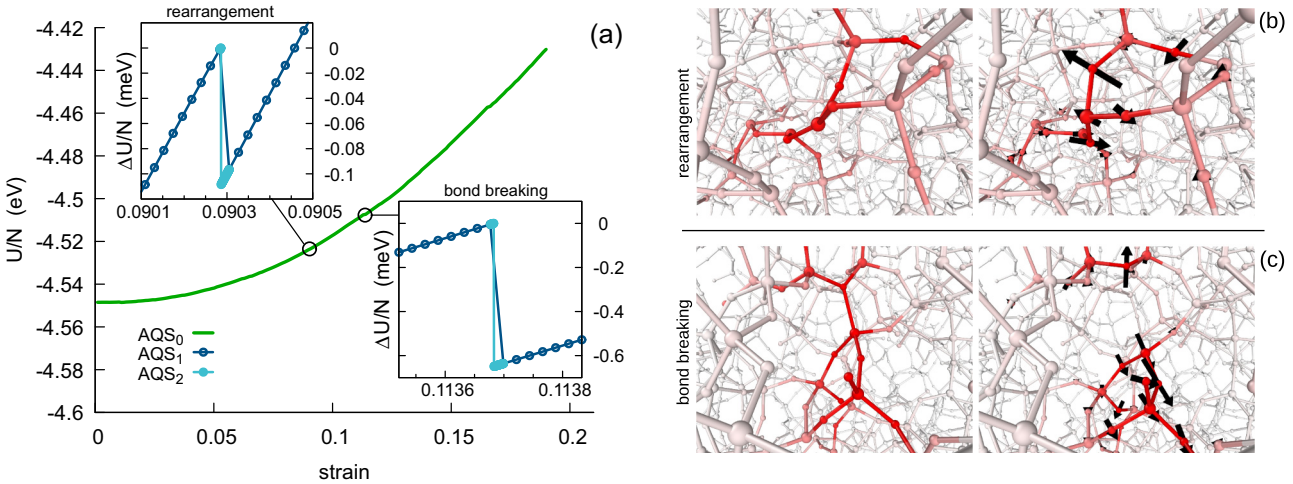

FIG. 1. (a) Typical dependence of potential energy per particle U/N on strain in the AQS_0 protocol for the three-dimensional (3D) silica glass. The insets are a blowup of two events emphasized by the circles on the main curve, the first being a localized rearrangement (top) and the second (bottom) reporting the first observed bond breaking (Si–O bond). Blue and light blue curves are obtained by decreasing strain step size, AQS_1 and AQS_2 respectively. The energy zero has been set to the maximum value before the drop, which is larger in the bond-breaking event. [(b), (c)] A 3D perspective view of the atomic positions before (left) and after (right) the energy drop for the corresponding events of panel (a). Large and small spheres represent Si and O atoms, respectively. Color and arrows report the magnitude of the occurred nonaffine atomic displacements. Arrows have been rescaled by a factor of 2. The corresponding movies are available in the Supplemental Material [19].

bonds which are absent in other well-studied amorphous systems.

In this paper, we study three-dimensional silica glass under AQS shear conditions. Previous numerical work [29] has shown that bond breaking is mainly responsible for damage accumulation and failure of silica at zero temperature. In this paper, we focus on the initial single events acting as fracture precursors and analyze the softest modes.

Models and methods. We perform simulations on a silica glass sample in a cubic box. The system is formed by a total of $N = 8250$ atoms, composed of $N_{Si} = 2750$ silicon atoms and $N_O = 5500$ oxygen atoms. Silica glasses are simulated using Watanabe's potential [30] with a similar sample preparation strategy. The advantage of this potential is that the usual Coulomb interaction term is implicitly replaced by a coordination-based bond softening function for Si-O atoms that accounts for the environmental dependence; therefore, we perform simulations in open boundary conditions to study surface effects. The general form of the potential consists of two terms: a two-body interaction that depends on distance and a three-body interaction that describe rotational and translational symmetry. The Hessian matrix [Eq. (1)] is computed numerically from the first-order derivatives of interparticle forces. To this extent, each element H_{ij} is obtained by calculating the force acting on particle i following a displacement of particle j by a small amount, $\delta = 10^{-7}$ Å along positive and negative directions and by applying the difference quotient. All the simulations have been performed using the LAMMPS simulator package [31] and visualized with the OVITO package [32].

To generate the sample, we have started from randomly positioned Si,O atoms, with density $\rho_{\text{in}} = 2.196$ g/cm^3 in a box size of $5\times5\times5$ nm^3. We then have applied the following annealing procedure: (i) After an initial 2 ps of Newtonian dynamics, with Lennard-Jones interatomic interactions viscously damped with a rate of 1/ps and atomic velocities limited to 1 Å/ps, we switch to our reference Watanabe's potential for silica [30] and (ii) we perform subsequent 8 ps of damped Newtonian dynamics. (iii) We then heat up the system up to 6000 K in 30 ps; (iv) thermalize at 6000 K for 80 ps; (v) reduce the temperature to 4000 K in 30 ps, (vi) then to 0.01 K in 50 ps, and (vii) then to 0.001 K in 100 ps; and (viii) finally we perform a pressure minimization—cell relaxation—for 50 ps. After such procedure, we get a final density $\rho_{fin} = 2.2439$ g/cm^3 and box size $4.948\times4.996\times4.948$ nm^3. Analysis on such initial sample compares well with experimentally observed density [33] and with previous calculations of atomic coordination [34].

The so-produced configuration is then used to start the AQS protocol. At each AQS step [14], we strain the sample along z and compress it along x and y according to a Poisson ratio $\nu = 0.17$. We have adopted three different increments of strain $\delta\gamma$, namely $\delta\gamma = 5\times10^{-4}$ (AQS_0), $\delta\gamma = (5\times10^{-4})/50$ (AQS_1), $\delta\gamma = (5\times10^{-4})/50/50$ (AQS_2). In order to reduce the computational burden, once a rearrangement event is identified in the faster AQS_0 simulation, we used the more refined AQS_1 and then AQS_2 simulations only in the vicinity of such event. After the imposed $\delta\gamma$ strain, an energy minimization through the fast inertial relaxation engine (FIRE) [35] scheme is performed until a maximum force of 10^{-10} eV/Å is reached.

Two types of events. In Fig. 1(a), the energy versus strain curve is reported. There we identify two events—marked by circles and magnified in the insets—which are of different nature, one associated to a typical quasilocalized rearrangement without any change in the atomic coordination, the other resulting from the first observed bond breaking. Thanks to these rearrangements, some of the internal stress is released, and a consequent drop in the energy occurs. As shown in the insets using the smaller $\delta\gamma$ values, both events manifest

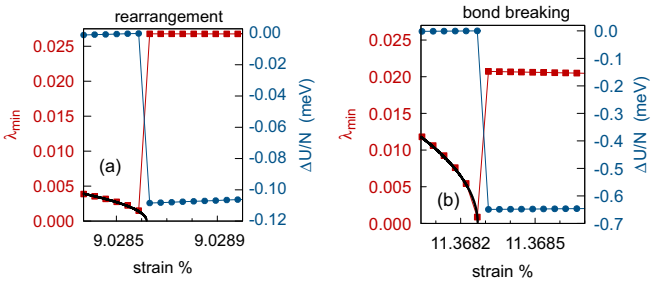

FIG. 2. Lowest eigenvalues and potential energy trend comparison for AQS_2 strain steps for (a) localized atomic rearrangement and (b) bond-breaking events. The lowest eigenvalue is reported in red squares and approaches zero at the critical strain $\gamma_c \simeq 9.02862\%$ and $\simeq 11.36827\%$, respectively. Black curve reports the fit $\lambda_{\min} \propto \sqrt{\gamma_c - \gamma}$. The energy drops are reported in blue dots.

a drop in the total energy, which results in about 0.9 and 5.4 eV for rearrangement and bond breaking, respectively, in line with previous works [27]. The nonaffine atomic displacements corresponding to the energy drops are represented in Figs. 1(b) and 1(c) (the corresponding movies are available in the Supplemental Material [19]). We note that while the rearrangement event consists in displacements along multiple directions, the bond breaking produces displacements mainly along the principal strain direction z. Specifically, the rearrangement involves changem in angle in two undercoordinated silicon atoms, and the bond breaking occurs between a Si and a O atom. Therefore, both events appear in the presence of a structural defect.

The number of particles involved in such fundamental nonaffine events can be estimated by the participation number $P_n = \sum_{i=1}^{N} (u_i/u_{\max})^2$, with u_i being the displacement modulus of atom i and $u_{\max}$ being the maximum u_i. Such calculation for rearrangement and bond-breaking events gives $P_n^{RR} = 3.73$ and $P_n^{BB} = 6.11$, respectively, revealing that the more energetic event involves, as expected, a larger effective number of particles. Furthermore, the participation ratio $P_r = \sum_{i=1}^{N} (\boldsymbol{e}_i \cdot \boldsymbol{e}_i)^2 / [\sum_{i=1}^{N} (\boldsymbol{e}_i \cdot \boldsymbol{e}_i)]^2$, calculated using the Hessian eigenvectors $\boldsymbol{e}_i$ right before the critical strain, results in $P_r^{RR} = 0.31$ and $P_r^{BB} = 0.20$.

Analytical investigation of the rearrangement events induced by external stress can be performed by computing the $\boldsymbol{H}$ matrix and by following the direction of the softest mode. The results of this investigation are reported in Fig. 2, showing that for both selected events the smallest eigenvalue $\lambda_{\min}$ progressively decreases following a square-root trend and vanishes at the critical strain value γ_c, marking a saddle point in the energy configuration space. As in the case of metallic glasses, governed by isotropic interactions, in which stress release is associated to a irreversible plastic event, we have verified that the same irreversibility occurs in the covalently bonded system under consideration. The application of a negative strain rate after a rearrangement does not follow the configurational path that led the system to that rearrangement.

Further information can be obtained by analyzing the eigenvectors associated with the lowest eigenvalue $\lambda_{\min}$, to be compared with the nonaffine displacement fields, calculated between the frame after the energy drop and the one before.

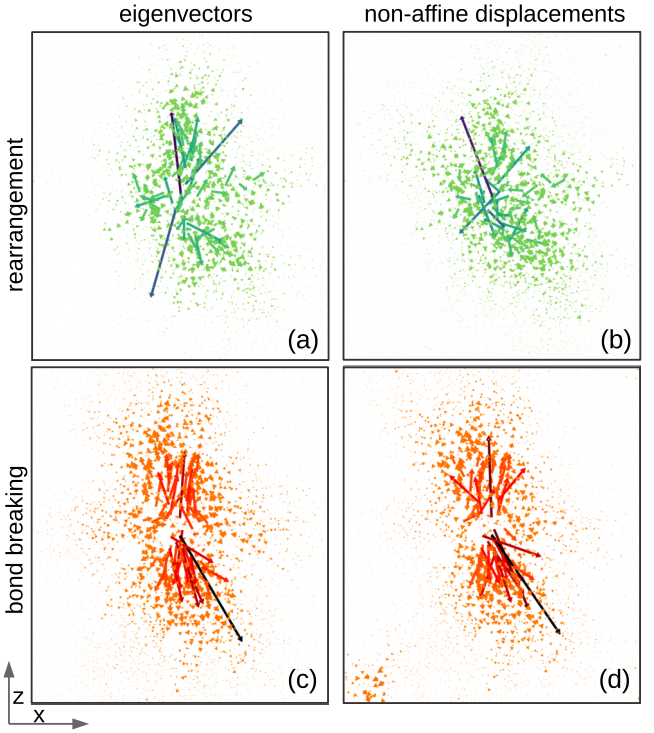

FIG. 3. Comparison between normalized nonaffine displacements (left) and eigenvectors (right) of the configuration before the bond breaking or energy drop (AQS_2 steps). Arrows are colored with respect to the modulus of the vectors. Arrows have been rescaled by a factor of 50, and the view is orthogonal. Panels (b) and (d) are related to Figs. 1(b) and 1(c), right panels.

In Fig. 3 we present such comparison for the selected plastic events showing an almost exact matching, especially in the case of bond breaking: The scalar products, $s = \sum_{i=1}^{N} (\boldsymbol{u}_i \cdot \boldsymbol{e}_i)$, of the normalized eigenvectors $\boldsymbol{e}_i$ and nonaffine displacements $\boldsymbol{u}_i$ are $s_{RR} \simeq 0.74$ and $s_{BB} \simeq 0.91$ respectively. The higher correlation in the latter case is likely due to the fact

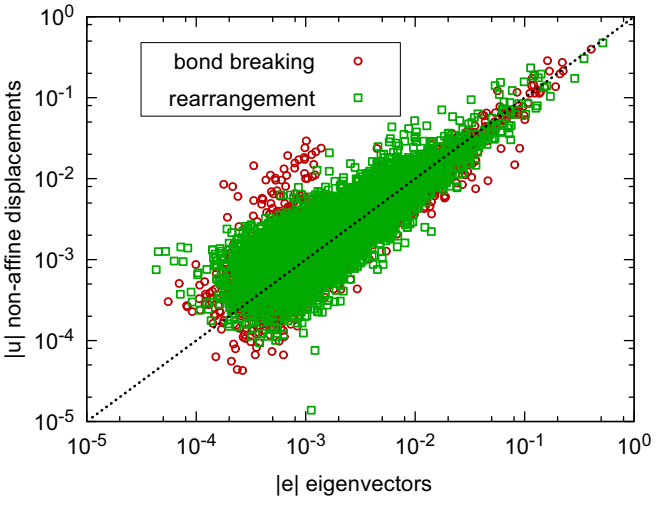

FIG. 4. Eigenvectors vs nonaffine displacement comparison for the rearrangement (squares) and bond-breaking (circles) events, compared to the ideal correlation line (dotted line).

that bond breaking occurs along the strain direction, while the rearrangement occurs through a local rotation of bonds, i.e., not connected to the strain direction. In any case, both mechanical events show a high correlation between the eigenvectors and displacements. This evidence is also supported by Fig. 4 in which the individual e_i versus u_i moduli are compared.

Concluding remarks and prospects. In summary, we have analyzed, using Hessian methods, the nature of nonaffine responses to mechanical shear strain in a model of silica. The difference from other examples of similar studies is that in silica we have *directional chemical bonds* between atoms, and these can be broken. In most models of glass formers, one cannot assign actual bonds, and one can even discuss glass physics with repulsive interaction only. The presence of bonds enriches that discussion of nonaffine responses to strain, offering plastic events that do not exist in most of the studied models of glass formers. We could therefore identify two distinctly different nonaffine responses in silica, one that corresponds to other models with so-called T1 processes that involves particles moving out and particles moving in on a quadrupolar quasilocalized structure, but also an elementary event of bond breaking. Both events are accompanied by an eigenvalue of the Hessian approaching zero with a square-root singularity and are associated with a stress and energy drop. Even in the case of bond breaking, the system response is again quadrupolar. This result is important for theoretical modeling of failure in real amorphous materials since our understanding of amorphous plasticity has often relied on mesoscale models assuming that plastic deformation can be decomposed into a series of discrete localized plastic instabilities [12]. While this assumption was supported by atomistic simulations in simplified isotropic models for glasses [17], the present study shows that the same description holds for more realistic anisotropic models. Finally, an important aspect of our findings is that by using the eigenfunction associated with the lowest eigenvalue one can predict the locus of the nonaffine response [36] even in realistic anisotropic conditions such as those simulated here.

Acknowledgments. This work is supported by the cooperation project COMPAMP/DISORDER jointly funded by the Ministry of Foreign Affairs and International Cooperation (MAECI) of Italy and by the Ministry of Science and Technology (MOST) of Israel.

[1] J. Horbach, W. Kob, K. Binder, and C. A. Angell, Finite size effects in simulations of glass dynamics, Phys. Rev. E **54**, R5897 (1996).

[2] D. Coslovich and G. Pastore, Dynamics and energy landscape in a tetrahedral network glass-former: Direct comparison with models of fragile liquids, J. Phys.: Condens. Matter **21**, 285107 (2009).

[3] P. Y. Huang, S. Kurasch, J. S. Alden, A. Shekhawat, A. A. Alemi, P. L. McEuen, J. P. Sethna, U. Kaiser, and D. A. Muller, Imaging atomic rearrangements in two-dimensional silica glass: Watching silica's dance, Science **342**, 224 (2013).

[4] A. S. Argon, Plastic deformation in metallic glasses, Acta Metall. **27**, 47 (1979).

[5] V. Chikkadi, G. Wegdam, D. Bonn, B. Nienhuis, and P. Schall, Long-Range Strain Correlations in Sheared Colloidal Glasses, Phys. Rev. Lett. **107**, 198303 (2011).

[6] M. Dennin, Statistics of bubble rearrangements in a slowly sheared two-dimensional foam, Phys. Rev. E **70**, 041406 (2004).

[7] P. Hébraud, F. Lequeux, J. P. Munch, and D. J. Pine, Yielding and Rearrangements in Disordered Emulsions, Phys. Rev. Lett. **78**, 4657 (1997).

[8] J. Clara-Rahola, T. A. Brzinski, D. Semwogerere, K. Feitosa, J. C. Crocker, J. Sato, V. Breedveld, and E. R. Weeks, Affine and nonaffine motions in sheared polydisperse emulsions, Phys. Rev. E **91**, 010301 (2015).

[9] J.-C. Baret, D. Vandembroucq, and S. Roux, Extremal Model for Amorphous Media Plasticity, Phys. Rev. Lett. **89**, 195506 (2002).

[10] Z. Budrikis and S. Zapperi, Avalanche localization and crossover scaling in amorphous plasticity, Phys. Rev. E **88**, 062403 (2013).

[11] Z. Budrikis, D. F. Castellanos, S. Sandfeld, M. Zaiser, and S. Zapperi, Universal features of amorphous plasticity, Nat. Commun. **8**, 15928 (2017).

[12] A. Nicolas, E. E. Ferrero, K. Martens, and J.-L. Barrat, Deformation and flow of amorphous solids: Insights from elastoplastic models, Rev. Mod. Phys. **90**, 045006 (2018).

[13] F. H. Stillinger, A topographic view of supercooled liquids and glass formation, Science **267**, 1935 (1995).

[14] C. E. Maloney and A. Lemaître, Amorphous systems in a thermal, quasistatic shear, Phys. Rev. E **74**, 016118 (2006).

[15] D. L. Malandro and D. J. Lacks, Relationships of shear-induced changes in the potential energy landscape to the mechanical properties of ductile glasses, J. Chem. Phys. **110**, 4593 (1999).

[16] H. G. E. Hentschel, S. Karmakar, E. Lerner, and I. Procaccia, Do athermal amorphous solids exist?, Phys. Rev. E **83**, 061101 (2011).

[17] R. Dasgupta, S. Karmakar, and I. Procaccia, Universality of the Plastic Instability in Strained Amorphous Solids, Phys. Rev. Lett. **108**, 075701 (2012).

[18] R. Dasgupta, H. G. E. Hentschel, and I. Procaccia, Microscopic Mechanism of Shear Bands in Amorphous Solids, Phys. Rev. Lett. **109**, 255502 (2012).

[19] See Supplemental Material at http://link.aps.org/supplemental/10.1103/PhysRevE.100.060602 for information on the Hessian matrix and movies related to Fig. 1.

[20] R. Dasgupta, O. Gendelman, P. Mishra, I. Procaccia, and C. A. B. Z. Shor, Shear localization in three-dimensional amorphous solids, Phys. Rev. E **88**, 032401 (2013).

[21] J. D. Eshelby, The determination of the elastic field of an ellipsoidal inclusion and related problems, Proc. R. Soc. London A **241**, 376 (1957).

[22] C. A. Angell, Perspective on the glass transition, J. Phys. Chem. Solids **49**, 863 (1988).

[23] M. L. Falk and J. S. Langer, Dynamics of viscoplastic deformation in amorphous solids, Phys. Rev. E **57**, 7192 (1998).

[24] A. Tanguy, F. Leonforte, and J.-L. Barrat, Plastic response of a 2D Lennard-Jones amorphous solid: Detailed analysis of the local rearrangements at very slow strain rate, Eur. Phys. J. E **20**, 355 (2006).

[25] M. L. Manning and A. J. Liu, Vibrational Modes Identify Soft Spots in a Sheared Disordered Packing, Phys. Rev. Lett. **107**, 108302 (2011).

[26] L. Gartner and E. Lerner, Nonlinear modes disentangle glassy and Goldstone modes in structural glasses, SciPost Phys. **1**, 016 (2016).

[27] P. Koziatek, J. L. Barrat, and D. Rodney, Short- and medium-range orders in as-quenched and deformed SiO_2 glasses: An atomistic study, J. Non-Cryst. Solids **414**, 7 (2015).

[28] J. Guo and J. C. Palmer, Fluctuations near the liquid-liquid transition in a model of silica, Phys. Chem. Chem. Phys. **20**, 25195 (2018).

[29] S. Bonfanti, E. E. Ferrero, A. L. Sellerio, R. Guerra, and S. Zapperi, Damage accumulation in silica glass nanofibers, Nano Lett. **18**, 4100 (2018).

[30] T. Watanabe, D. Yamasaki, K. Tatsumura, and I. Ohdomari, Improved interatomic potential for stressed Si, O mixed systems, Appl. Surf. Sci. **234**, 207 (2004).

[31] S. Plimpton, Fast parallel algorithms for short-range molecular dynamics, J. Comp. Phys. **117**, 1 (1995).

[32] A. Stukowski, Visualization and analysis of atomistic simulation data with ovito–the open visualization tool, Modell. Simul. Mater. Sci. Eng. **18**, 015012 (2009).

[33] R. Brueckner, Properties and structure of vitreous silica. I, J. Non-Cryst. Solids **5**, 123 (1970).

[34] K. Vollmayr-Lee and A. Zippelius, Temperature-dependent defect dynamics in the network glass SiO_2, Phys. Rev. E **88**, 052145 (2013).

[35] E. Bitzek, P. Koskinen, F. Gähler, M. Moseler, and P. Gumbsch, Structural Relaxation Made Simple, Phys. Rev. Lett. **97**, 170201 (2006).

[36] S. Karmakar, A. Lemaître, E. Lerner, and I. Procaccia, Predicting Plastic Flow Events in Athermal Shear-Strained Amorphous Solids, Phys. Rev. Lett. **104**, 215502 (2010).